Three-Dimensional Instabilities in Tornado-like Vortices with Secondary Circulations

Or:

"Another look at the multiple vortex phenomenon"

David S. Nolan

Rosenstiel School of Marine and Atmospheric Sciences
University of Miami
Miami, Florida

I. Multiple Vortices in Tornadoes

- Tornadic vortices are frequently seen to exhibit "multiple vortices."

These structures can appear on a range of scales:

"multiple-vortex tornado"

Figure 4
An example of a multiple-vortex tornado. Photograph courtesy of H.B. Bluestein.

(from Rotunno 2013)

"suction vortices"

Figure 1. Ellis County, OK tornado of May 4, 2007. Photos courtesy of Reed Timmer and Joel Taylor of TornadoVideos.net. Image (a) is from approximately 1 km away, a few minutes before the viewing at approximately 100 m in the (b) image. Suction vortices are evident at the base of the condensation funnel.

(from Fiedler 2009)

II. Prior Work

- What are the mechanics of this instability? How does it extract energy?

We often try to answer such questions by linearized stability analysis:

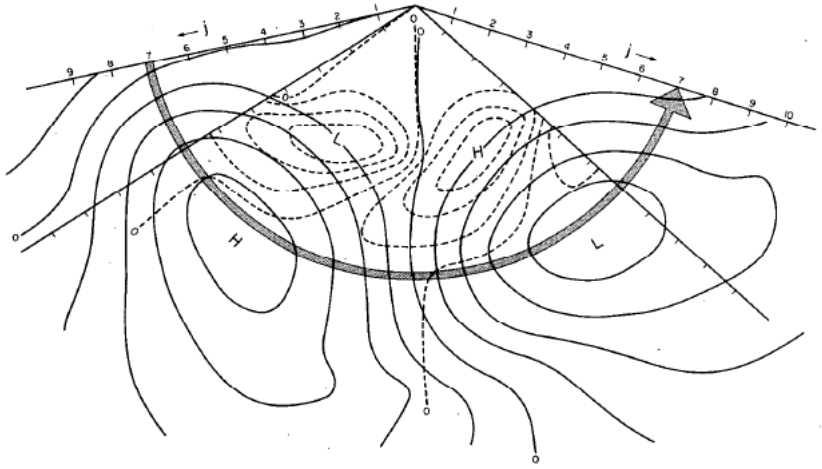

FIG. 7. Structure of the two most unstable modes at the 45.7 m level. Dashed curves show ψ for $n=3.4$ and the mode (inner) resulting from departure from $V=$constant $\times r$ inside the wind maximum (see curves a in Fig. 4). Solid curves show ψ for $n=2.4$ and the mode (outer) resulting from departure from $V=K/r$ outside the wind maximum (see curves b in Fig. 4). Units are arbitrary. Radial distance is indicated by the index j, with maximum wind, as indicated by the large curved arrow, at $j=7$.

Staley and Gall (1979)

$$v(r,\lambda,z,t) = V(r) + v_n(r)e^{i(n\lambda-\omega t)}$$

$$u(r,\lambda,z,t) = \quad u_n(r)e^{i(n\lambda-\omega t)}$$

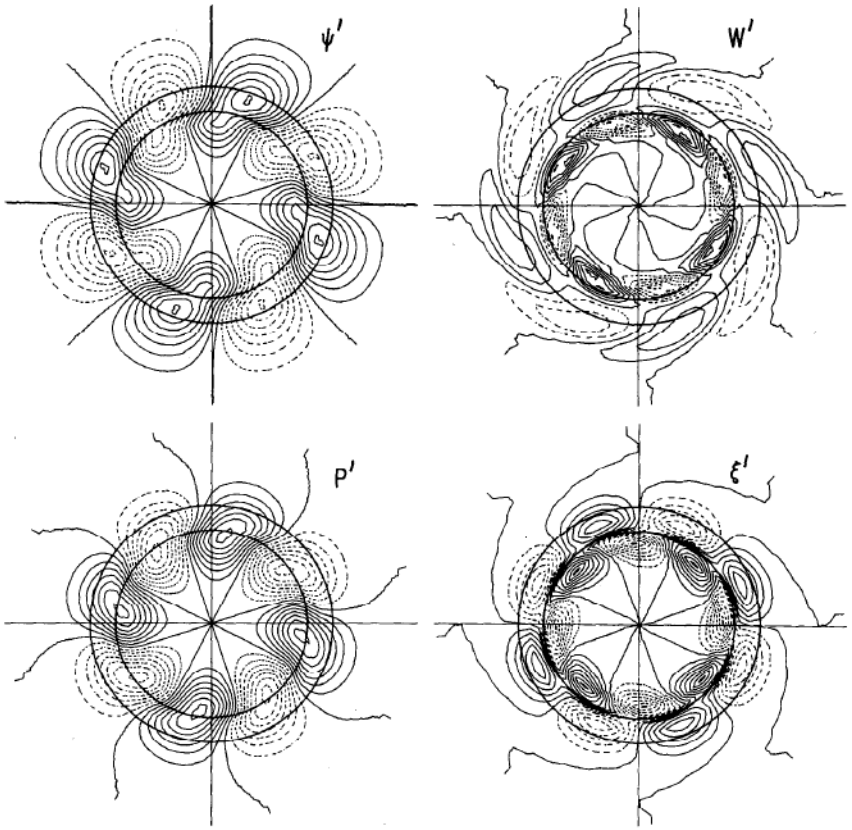

FIG. 8. As in Fig. 5 but for azimuthal wavenumber 4, vertical wavelength 200 cm, and swirl ratio $S = 1.4$.

Gall (1983)

$$v(r,\lambda,z,t) = V(r) + v_n(r)e^{i(kz+n\lambda-\omega t)}$$

$$u(r,\lambda,z,t) = \quad u_n(r)e^{i(kz+n\lambda-\omega t)}$$

$$w(r,\lambda,z,t) = W(r) + w_n(r)e^{i(kz+n\lambda-\omega t)}$$

Walko and Gall (1984):

$$u(r, \lambda, z, t) = U(r, z) + u_n(r, z)e^{i(n\lambda - \omega t)},$$
$$v(r, \lambda, z, t) = V(r, z) + v_n(r, z)e^{i(n\lambda - \omega t)},$$
$$w(r, \lambda, z, t) = W(r, z) + w_n(r, z)e^{i(n\lambda - \omega t)}.$$

Basic-State Flow from Axisymmetric Model

U V W

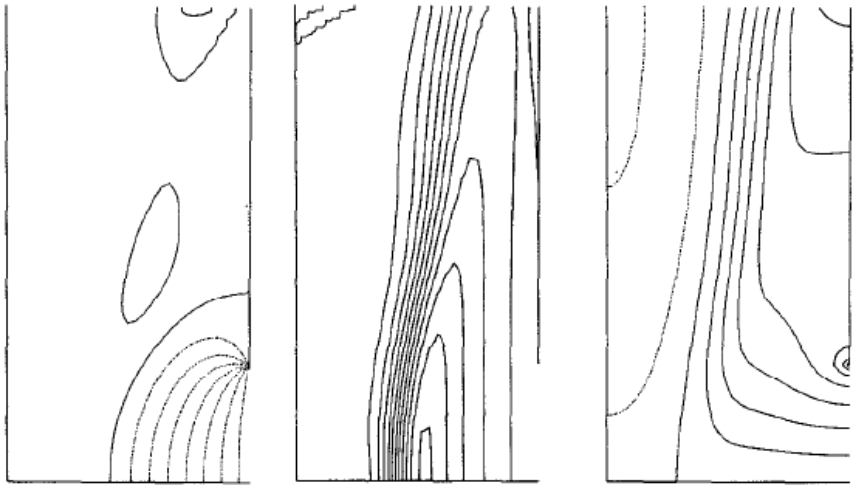

FIG. 2. Radial–height cross sections showing, from left to right, the radial, azimuthal, and vertical components of the steady-state axisymmetric velocity field for $S = 1.0$ and $\nu = 10.0$ cm^2 s^{-1}. The center axis of the TVC corresponds to the left edge of each picture, and the inflow port is indicated on the right. Dashed contours represent negative values, with zero corresponding to the first solid line. The contour intervals for the pictures are 0.04, 0.05 and 0.1, respectively, in m s^{-1}.

3D Modes with Vertical Structure

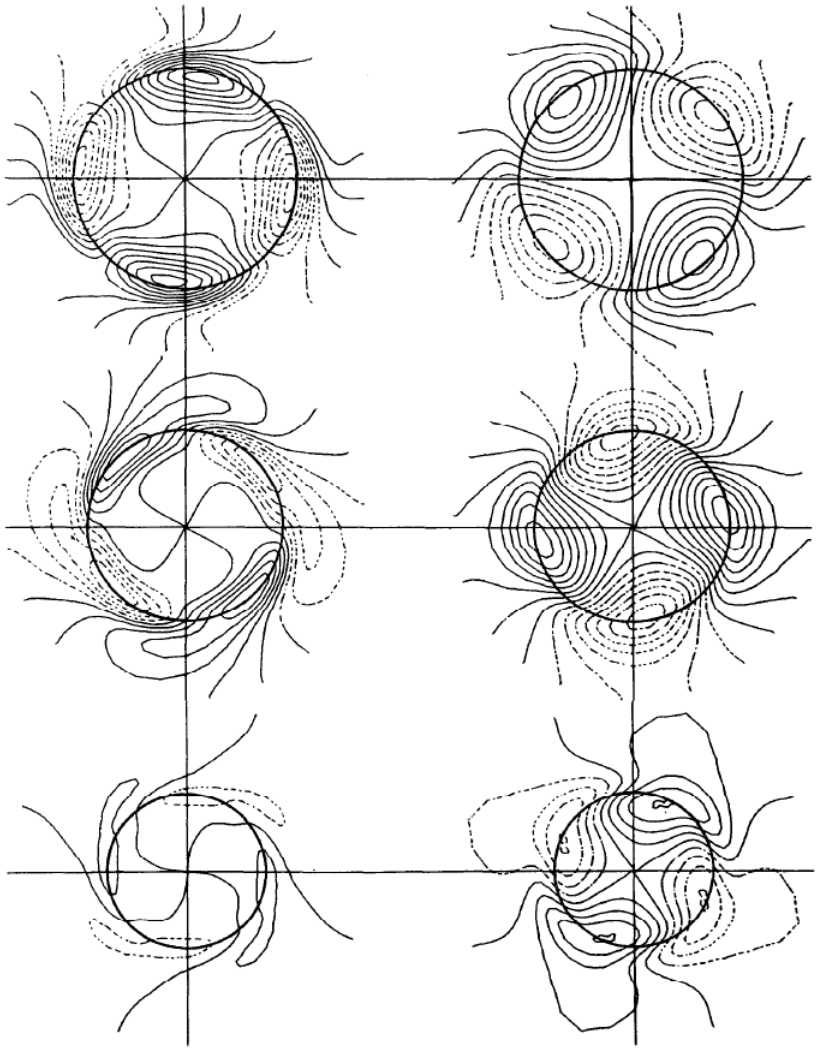

FIG. 7. As in Fig. 6 but showing w' (left column) and p' for the same case. The contour interval for w' is the same as that used for u' and v', and p' uses the same contour interval at all levels.

- The Walko and Gall (1984) energy analysis shows how the modes vary with wavenumber and swirl:

$$\frac{\partial}{\partial t}\iiint E' r dr d\theta dz = \iiint \left\{ \left[u'v' \left(\frac{\bar{v}}{r} - \frac{\partial \bar{v}}{\partial r} \right) \right]_1 + \left(-u'w' \frac{\partial \bar{w}}{\partial r} \right)_2 + \left(-u'u' \frac{\partial \bar{u}}{\partial r} - v'v'\bar{u} \right)_3 \right.$$
$$+ \left(-v'w' \frac{\partial \bar{v}}{\partial z} \right)_4 + \left(-w'w' \frac{\partial \bar{w}}{\partial z} \right)_5 + \left(-w'u' \frac{\partial \bar{u}}{\partial z} \right)_6$$
$$\left. + (u'F'_r + v'F'_\theta + w'F'_z)_8 \right\} r dr d\theta dz + \iint \{ [(-\bar{w}E')_{\mathrm{TOP}}]_7 + [(-p'w'/\rho)_{\mathrm{TOP}}]_9 \} r dr d\theta.$$

low swirl --> energy comes from (2): dW/dr

high swirl --> energy comes from (1): dV/dr

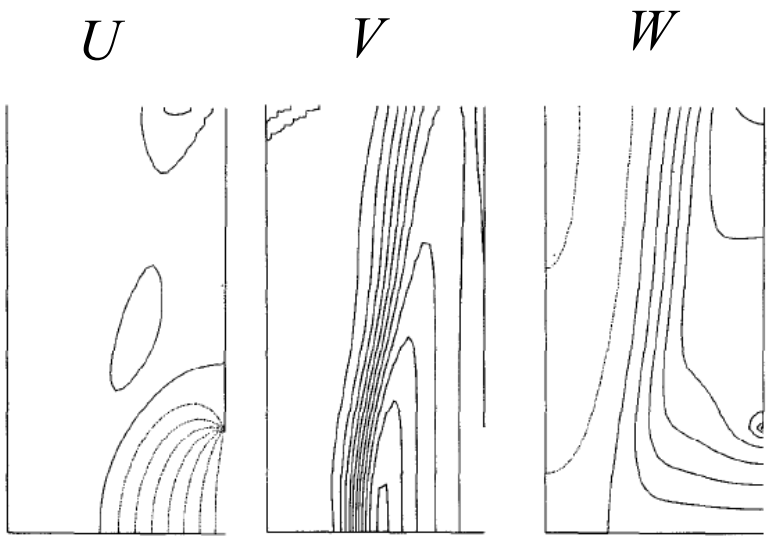

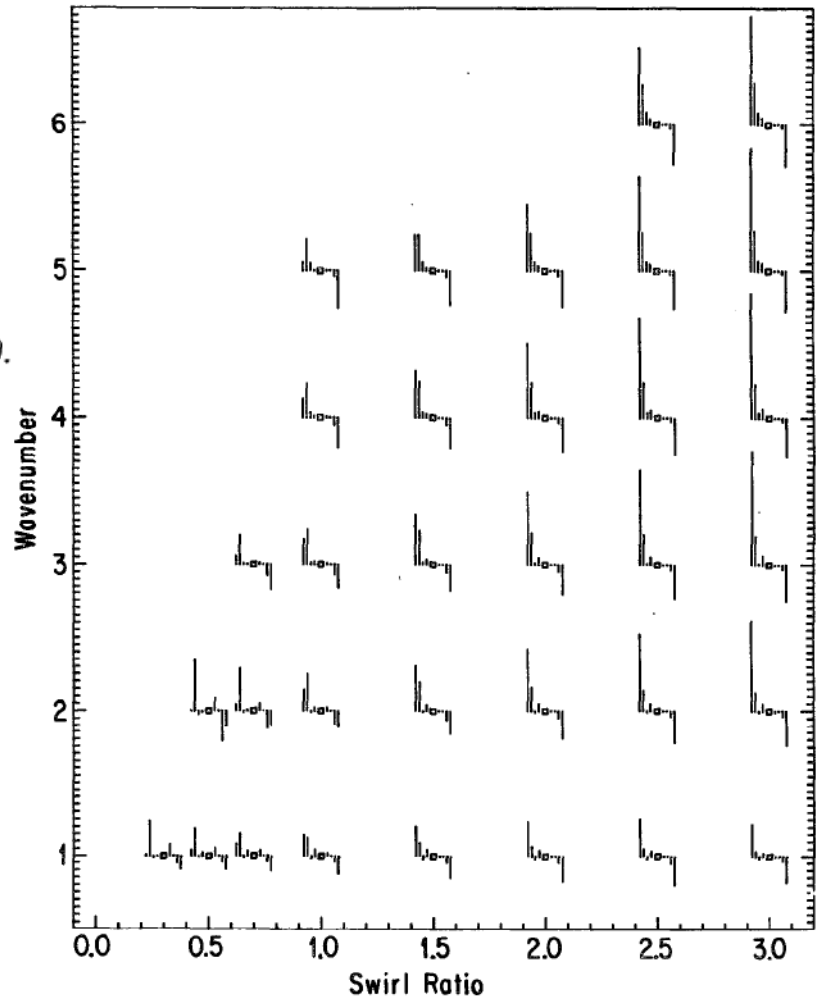

FIG. 9. Histograms showing the contributions of eight individual sources (or sinks) of energy for the linear perturbations as a function of swirl ratio and wavenumber. The small square within each histogram serves to locate the proper positions on the coordinate axes. The height of any bar indicates the contribution to the total perturbation growth rate with the small increments on vertical axis denoting units of 0.1 s^{-1}.

But - WG84 used a free-slip lower BC. No inflow jet, no localized wind max.

- What came next?

This paper (1984) was the last to study modes in a vertically varying vortex!

Some questions:

* Are the modes similar if we have a more realistic boundary layer?

* WG84 is a stability analysis of asymmetric modes on an axisymmetric flow. What if we use the time-mean of a 3D simulation instead?

* What about symmetric modes?

- We seek to perform a fully "self-consistent" stability analysis of the time-mean of a 3D tornado-like vortex, with a frictional boundary layer and secondary circulation.

III. Basic-State Flows

- For *U*, *V*, and *W*, we use time-azimuthal mean flows from the more recent three-dimensional simulations by Brian Fiedler (2009):

one-celled vortex

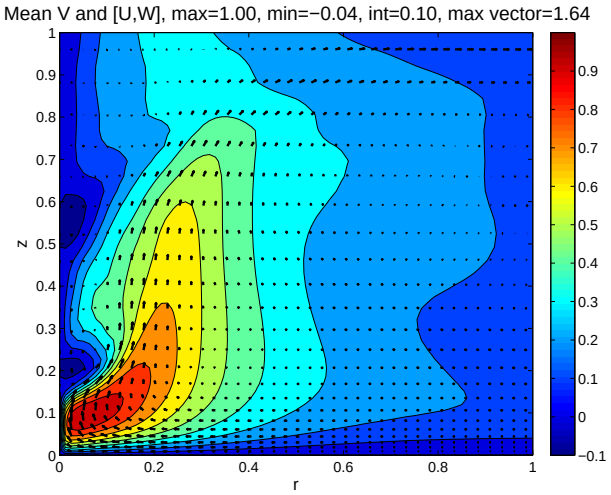

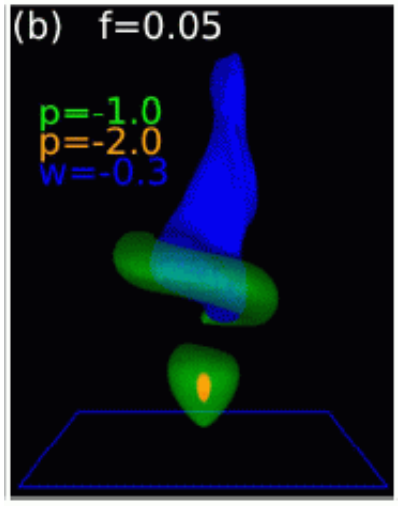

$\nu = 0.0004$

drowned vortex jump (DVJ)

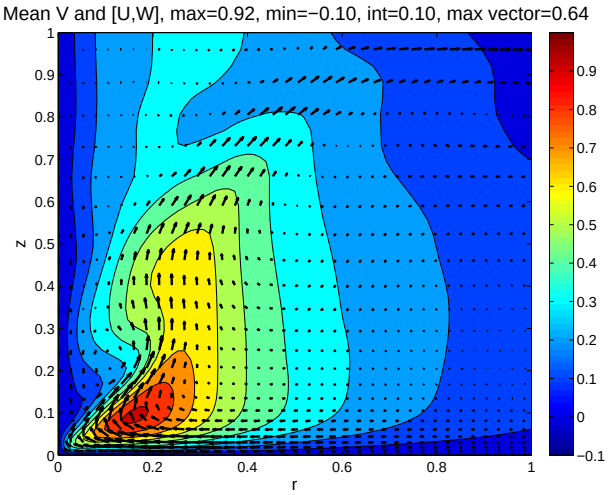

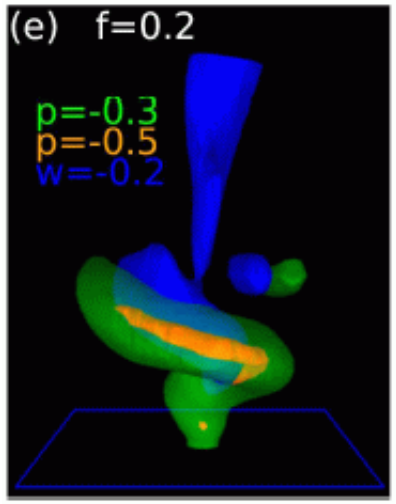

$\nu = 0.0004$

two-celled vortex

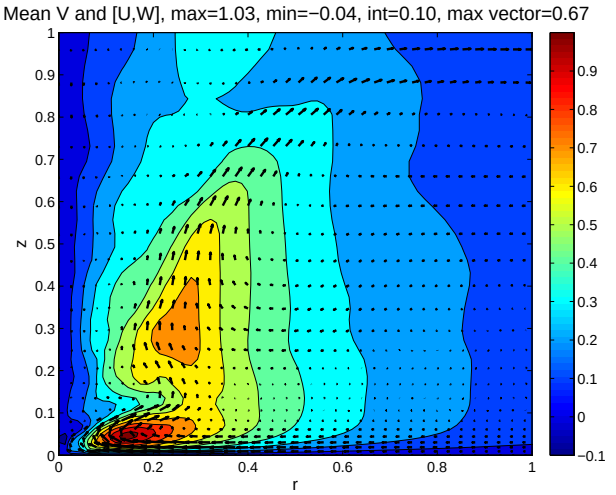

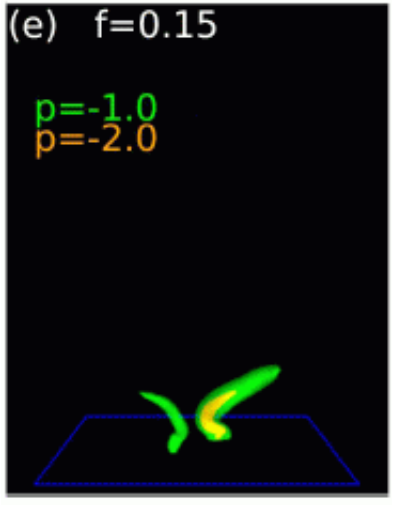

$\nu = 0.0001$

IV. Linearization and Discretization

- The incompressible equations of motion are linearized about the mean states $U(r,z), V(r,z), W(r,z)$ to make linear equations for u_n, v_n, w_n, p_n.

- The equations are discretized by finite differences on stretched, staggered grids:

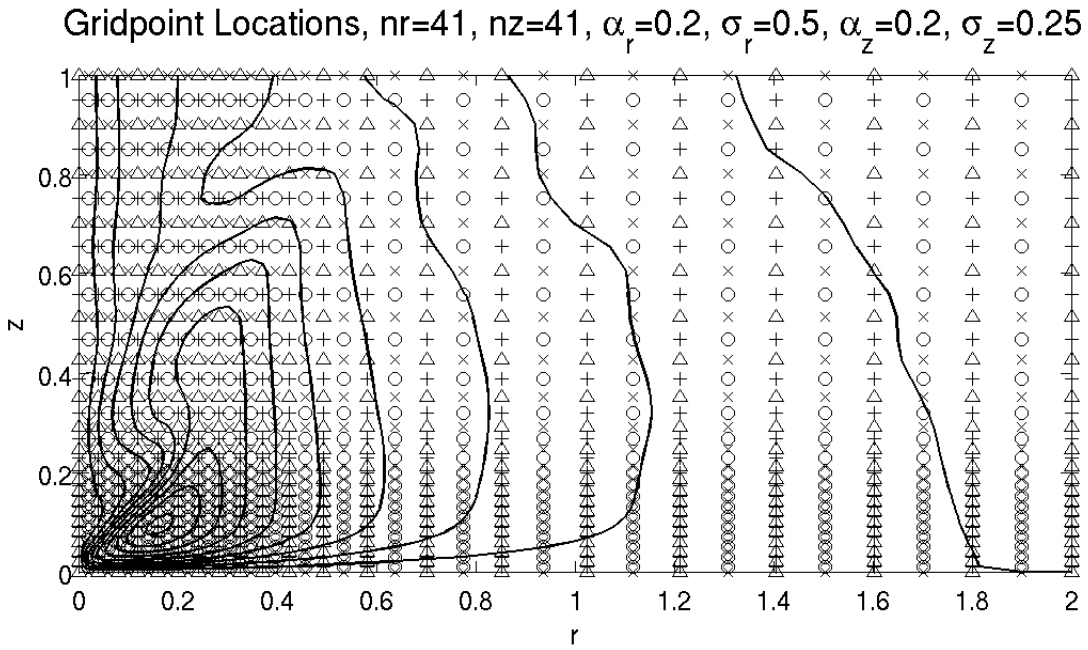

leading to the linear dynamical systems:

$$\text{asymmetric} \dashrightarrow \frac{d}{dt}\begin{bmatrix} u_n \\ w_n \end{bmatrix} = \mathbf{T}_n \begin{bmatrix} u_n \\ w_n \end{bmatrix} \quad \text{and} \quad \frac{d}{dt}\begin{bmatrix} \psi_0 \\ v_0 \end{bmatrix} = \mathbf{T}_0 \begin{bmatrix} \psi_0 \\ v_0 \end{bmatrix} \dashleftarrow \text{symmetric}$$

(complex) (real)

V. Results

- For each matrix $\mathbf{T}_n$, Matlab can provide all the eigenvalues and eigenvectors, each of which evolves as:

$$v(r, z, \lambda, t) = v_n(r, z)e^{st}e^{in\lambda} \text{ where } s \text{ is the complex eigenvalue } (s \leftrightarrow -i\omega)$$

so eigenvalues with largest real part indicate the "most unstable mode."

weak symmetric instability

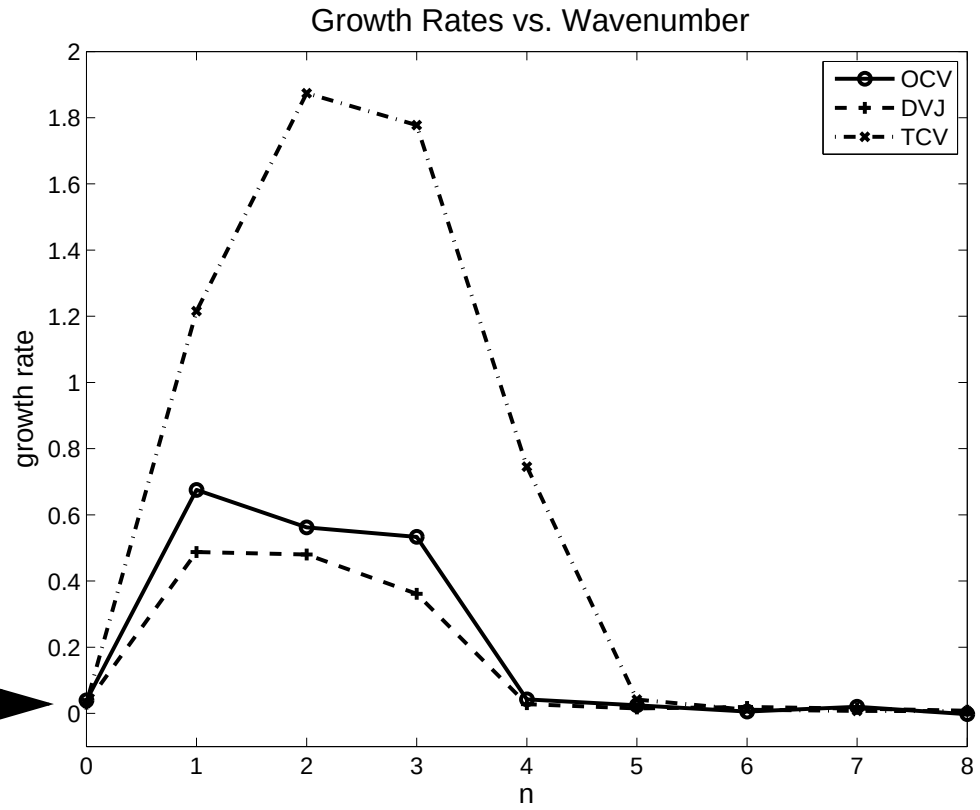

Most Unstable Mode: One-Celled Vortex

(perturbation pressure shows axes of vortical motion)

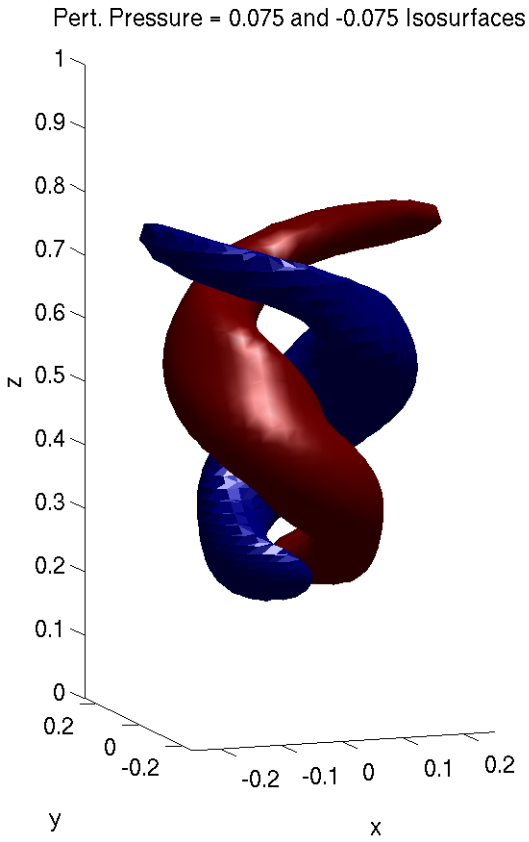

$n = 1$

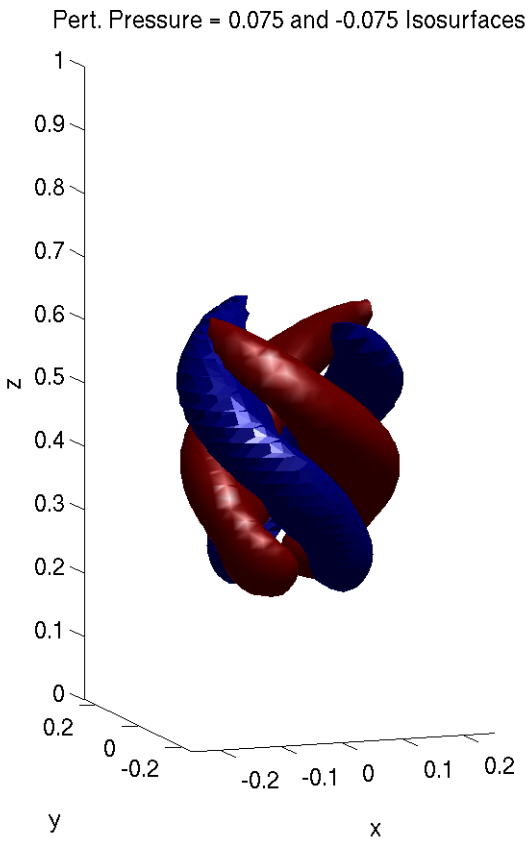

$n = 2$

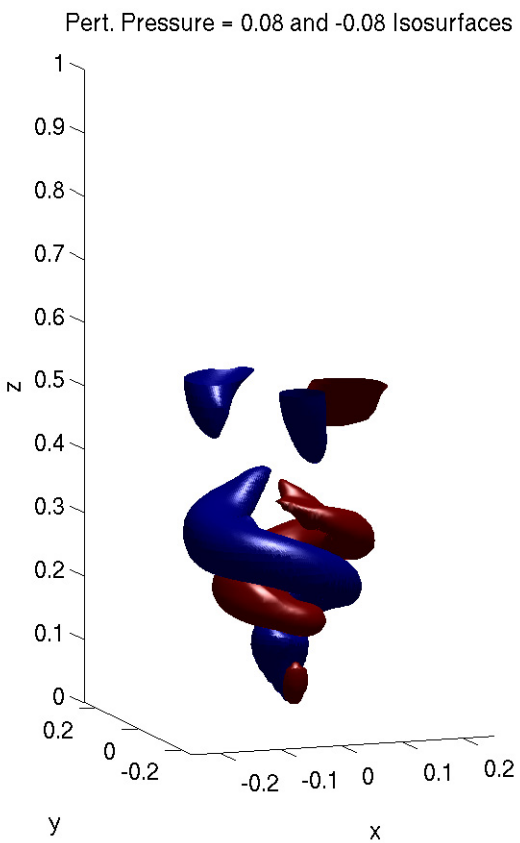

from nonlinear simulation

- Results: $n = 1$ is the dominant asymmetry

  $n = 2$ is close behind, so may occasionally appear

  Upward flow is supercritical: asymmetric modes can not reach the surface!

Most Unstable Modes: Drowned Vortex Jump

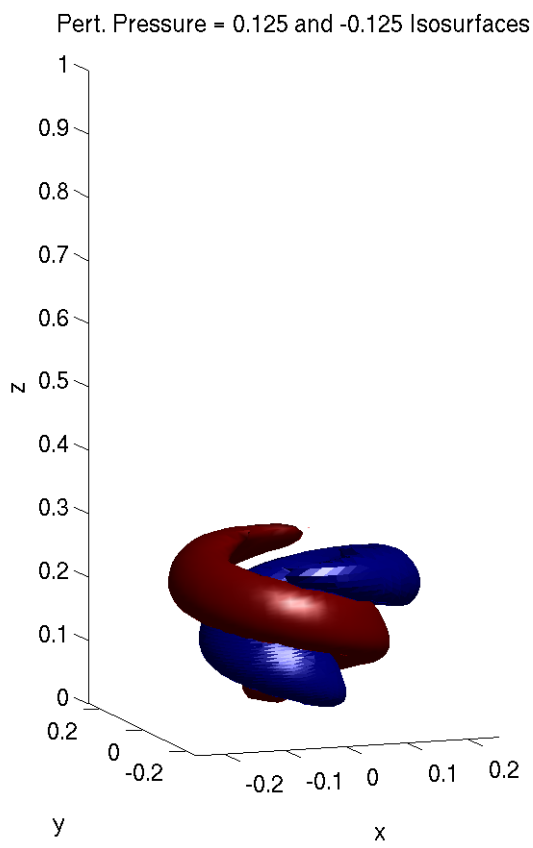

$n = 1$

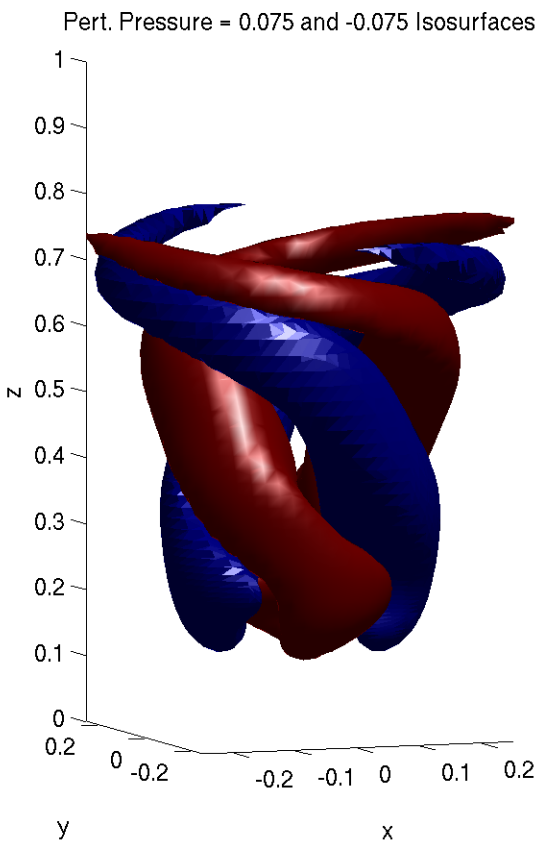

$n = 2$

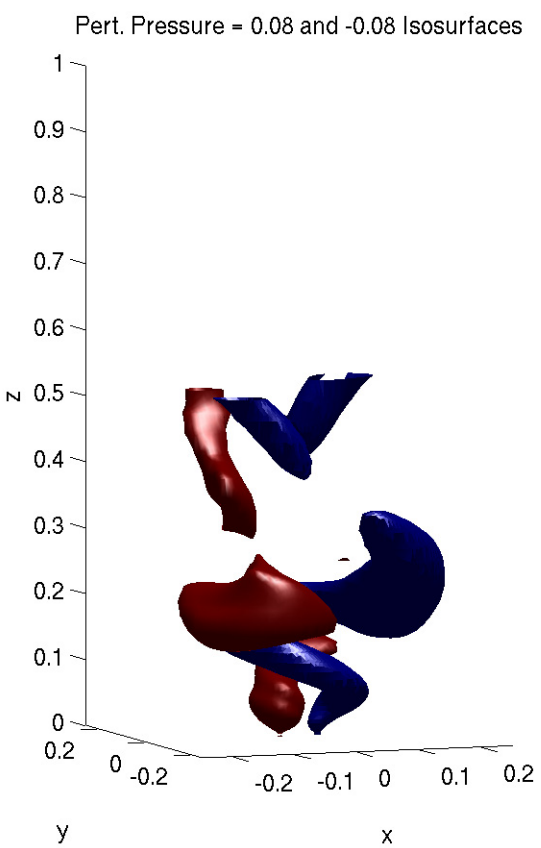

from nonlinear simulation

- Results: low-level $n = 1$ mode dominates, and causes vortex "wandering"

  Some $n = 2$ activity aloft.

  $n = 2$ shows transition from "barotropic" to "spiral" structure.

Most Unstable Modes: Two-Celled Vortex

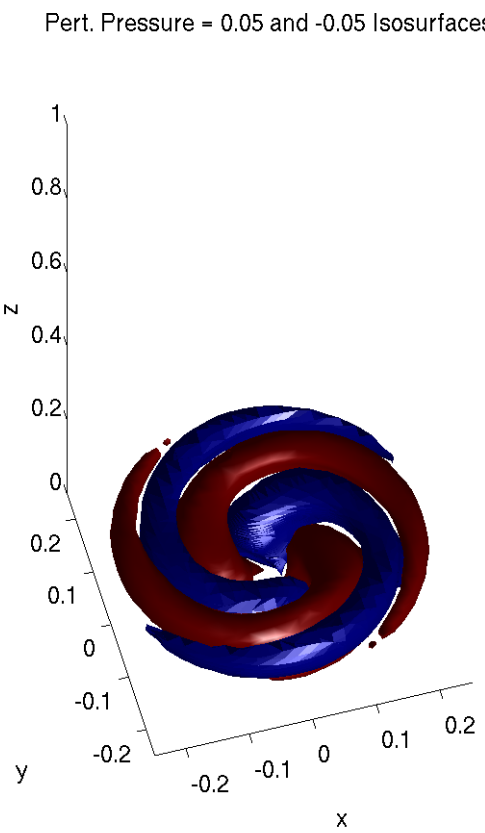

$n = 2$

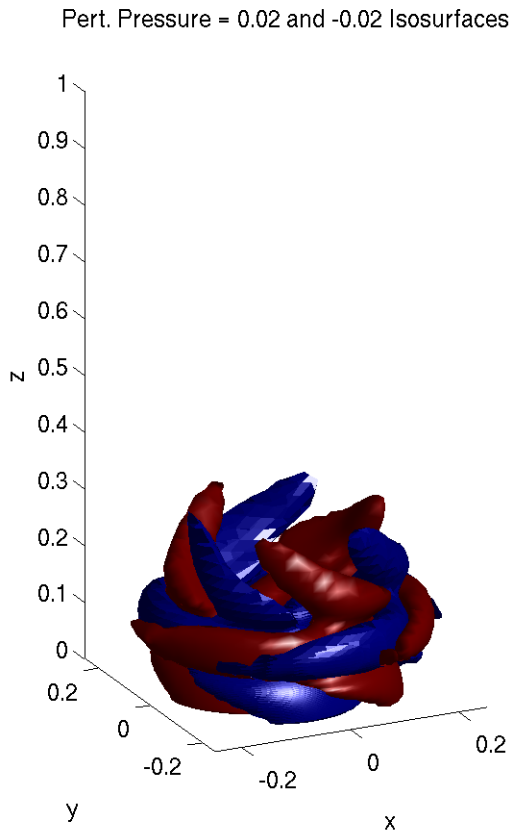

$n = 3$

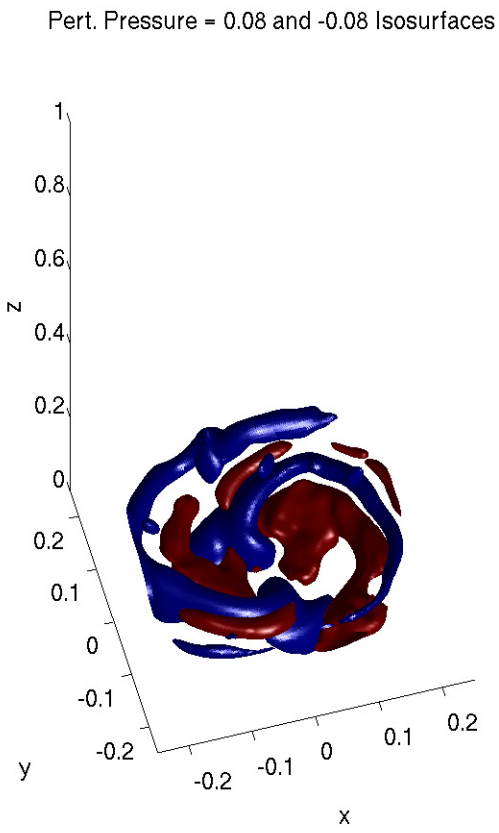

from nonlinear simulation

- Results: $n = 2$ mode dominates with “low and tight” spirals

Mode Energetics

- We can derive an equation for perturbation kinetic energy change:

$$\frac{\partial E'}{\partial t} = -\iint\left\{\left[\overline{u'v'}\left(\frac{\partial \bar{v}}{\partial r}-\frac{\bar{v}}{r}\right)\right]_{vr}+\left[\overline{u'w'}\frac{\partial \bar{w}}{\partial r}\right]_{wr}+\left[\overline{u'u'}\frac{\partial \bar{u}}{\partial r}+\overline{v'v'}\frac{\bar{u}}{r}\right]_{ur}+\right.$$

$$\left.\left[\overline{v'w'}\frac{\partial \bar{v}}{\partial z}\right]_{vz}+\left[\overline{w'w'}\frac{\partial \bar{w}}{\partial z}\right]_{wz}+\left[\overline{u'w'}\frac{\partial \bar{u}}{\partial z}\right]_{uz}+[\overline{u'F_r'}+\overline{v'F_\lambda'}+\overline{w'F_z'}]_F\right\}2\pi r\,dr\,dz$$

Each of these terms is a momentum flux across a wind shear.

If we integrate by parts, we can find a more intuitive form:

$$\frac{\partial E'}{\partial t} = \iint\left\{\left[\bar{v}\frac{1}{r^2}\frac{\partial}{\partial r}(\overline{r^2u'v'})\right]_{vr}+\left[\bar{w}\frac{1}{r}\frac{\partial}{\partial r}(\overline{ru'w'})\right]_{wr}+\left[\bar{u}\left(\frac{\partial}{\partial r}(\overline{u'u'})+\frac{\overline{v'v'}}{r}\right)\right]_{ur}+\right.$$

$$\left.\left[\bar{v}\frac{\partial}{\partial z}(\overline{v'w'})\right]_{vz}+\left[\bar{w}\frac{\partial}{\partial z}(\overline{w'w'})\right]_{wz}+\left[\bar{u}\frac{\partial}{\partial z}(\overline{u'w'})\right]_{uz}+[\overline{u'F_r'}+\overline{v'F_\lambda'}+\overline{w'F_z'}]_F\right\}2\pi r\,dr\,dz$$

Each of these terms is a eddy tendency (by the waves) acting on a mean velocity:

$$\frac{\partial E'}{\partial t}\sim-\frac{\partial \bar{E}}{\partial t}\sim-\left[\bar{v}\times\left\{-\frac{1}{r^2}\frac{\partial}{\partial r}(\overline{r^2u'v'})\right\}\right]$$

We can plot the dominant energy terms for modes of interest:

n = 1, one-celled

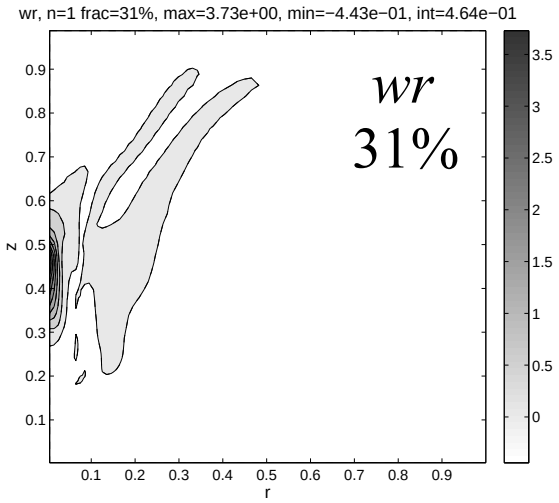

n = 2, DVJ

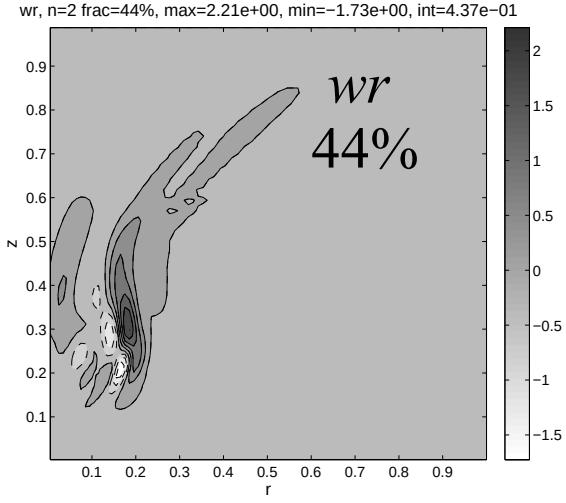

n = 2, two-celled

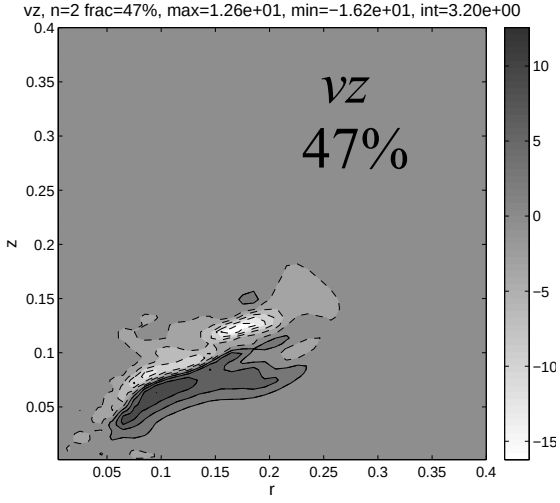

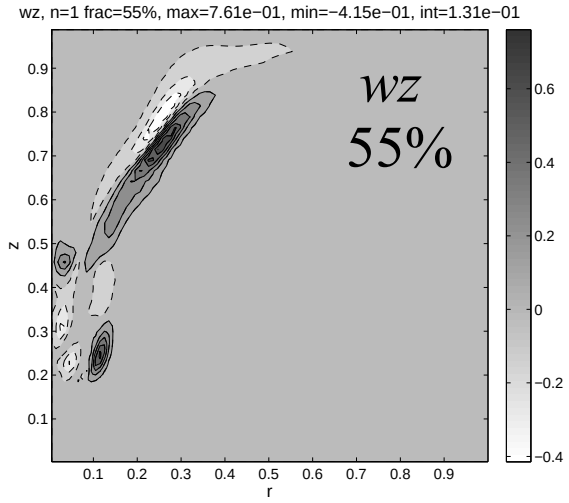

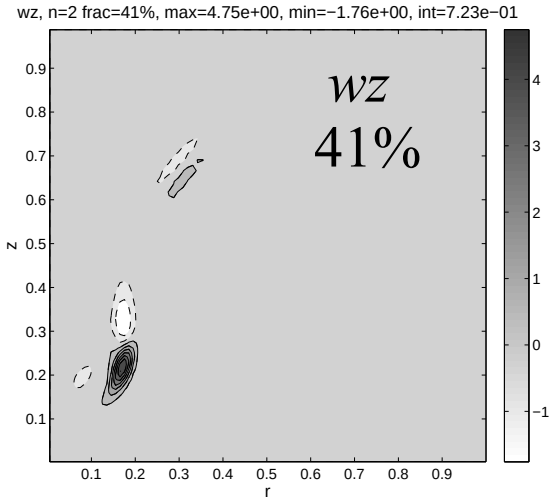

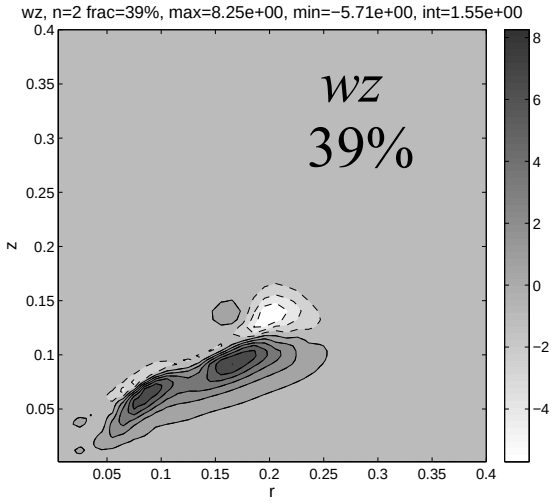

- Results: The *wr* and *wz* terms are the dominant energy source for asymmetric modes.

  vz also large for the two-celled vortex.

  The radial shear of tangential wind is never significant! (max 1.4%)

Symmetric Modes

```
>> load F09_onecell_R2/F09_161x161n0
>> s

s =

   0.0392 + 0.5312i

>> sm

sm =

   0.0392 + 0.5312i
   0.0392 - 0.5312i
   0.0322 + 0.2930i
   0.0322 - 0.2930i
   0.0307 + 0.7483i
   0.0307 - 0.7483i
   0.0211
   0.0098 + 0.9522i
   0.0098 - 0.9522i
  -0.0061 + 1.1539i
  -0.0061 - 1.1539i
  -0.0073
  -0.0124 + 1.3434i
  -0.0124 - 1.3434i
  -0.0200 + 1.4906i
  -0.0200 - 1.4906i
  -0.0427 + 0.0221i
  -0.0427 - 0.0221i
  -0.0494 + 0.3537i
  -0.0494 - 0.3537i
```


Most unstable eigenvalue

First 20 eigenvalues

- The complex modes are always matched with a complex conjugate. The imaginary parts always exactly cancel.

But, the *structure* of the symmetric mode evolves in time:

$$v_n \sim Re\{v_n\} \rightarrow Im\{v_n\} \rightarrow -Re\{v_n\} \rightarrow -Im\{v_n\}.$$

real[v_0] and real[u_0,w_0], max=6.8e−01, min=−1.0e+00, int=1.0e−01 maxvec=8.5e−01

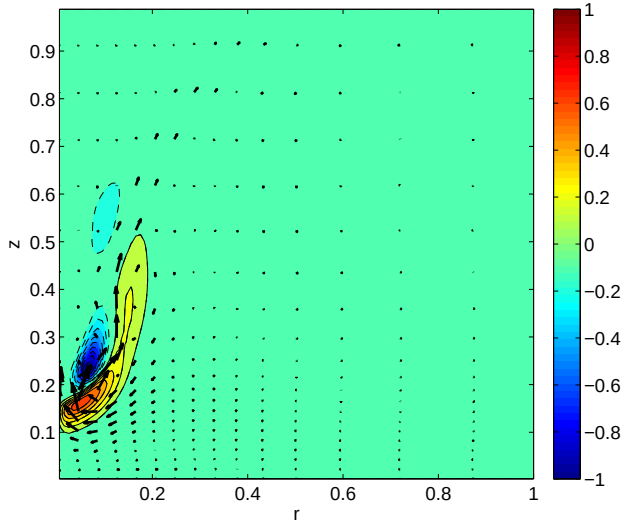

imag[v_0] and imag[u_0,w_0], max=6.8e−02, min=−1.2e−01, int=1.0e−01 maxvec=2.3e−01

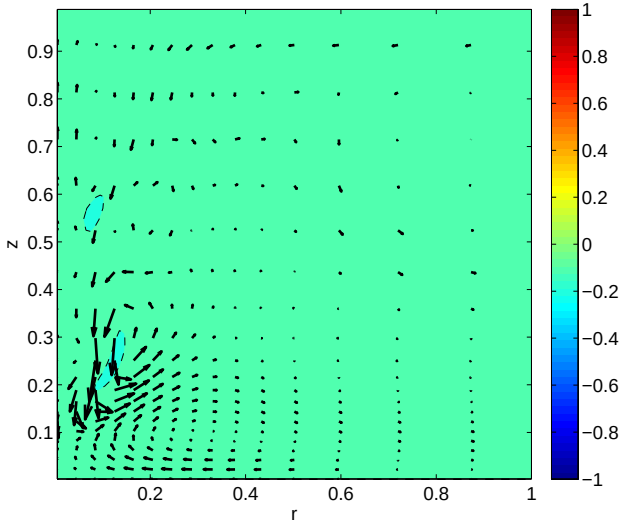

−real[v_0] and −real[u_0,w_0], max=1.0e+00, min=−6.8e−01, int=1.0e−01 maxvec=8.5e−01

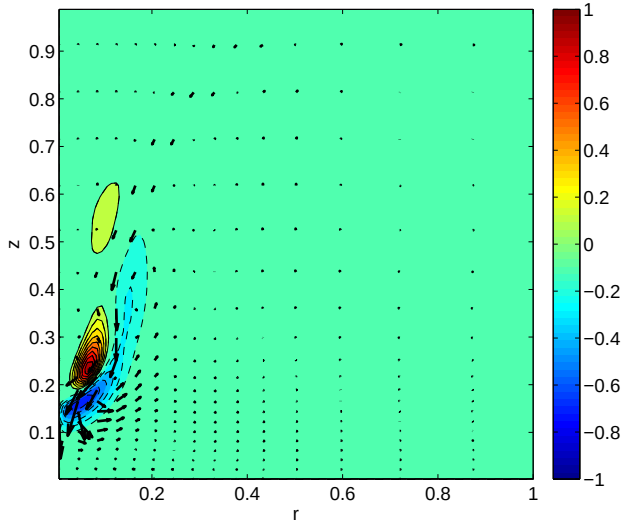

-imag[v_0] and −imag[u_0,w_0], max=1.2e−01, min=−6.8e−02, int=1.0e−01 maxvec=2.3e−01

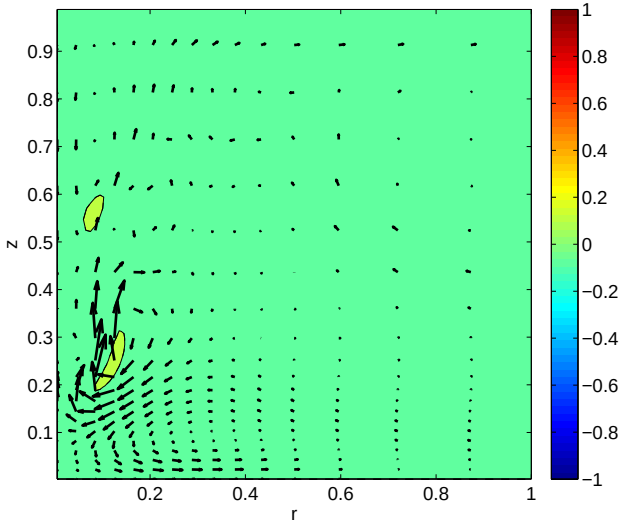

These modes represent *symmetric oscillations* of the inner-core.

Bluestein et al. (2003, MWR)

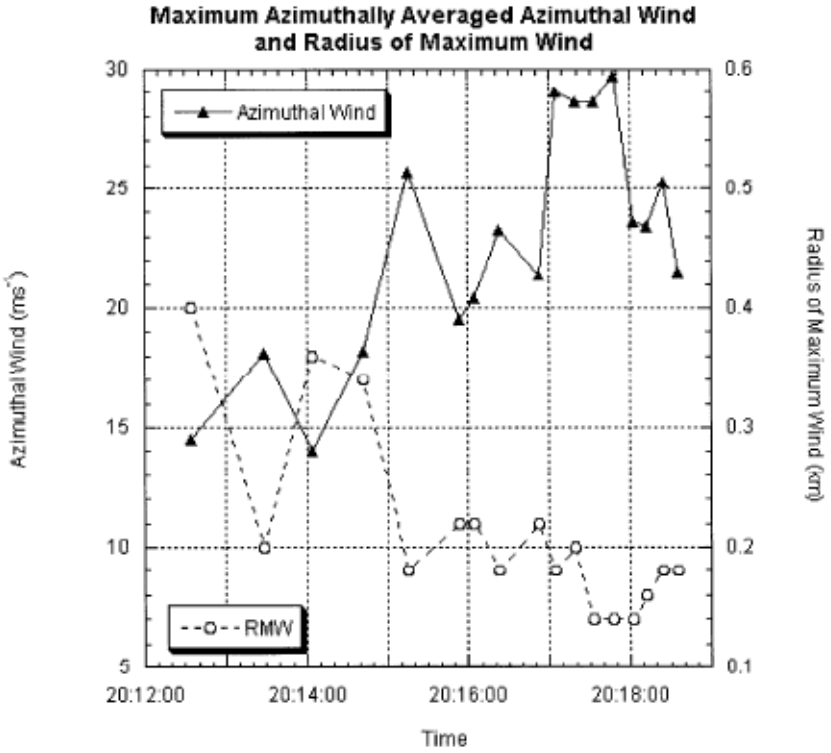

Tanamachi et al. (2007, MWR)

FIG. 1. The UMass W-band radar collecting data in the Stockton, KS, tornado. The view is to the northwest, and the truck is facing east. (Photograph courtesy of H. Bluestein.)

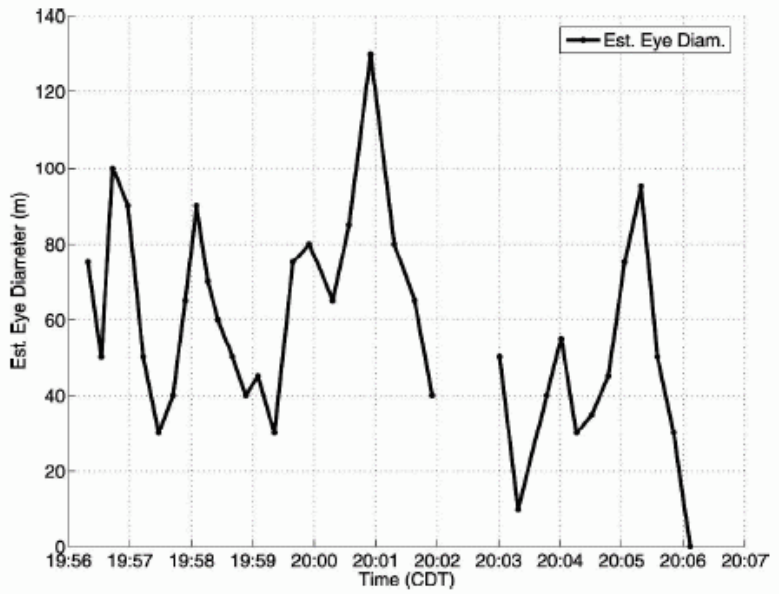

FIG. 6. Estimated diameter (m) of the low-reflectivity eye of the Stockton tornado as a function of time.

- How can we tell if our symmetric modes are similar to the observed?

One way is to compare time scales.

One-celled vortex: circulation time scale $= \tau_{circ} = \frac{2\pi \times \mathrm{RMW}}{V_{max}} = \frac{2\pi \times 0.05}{1.0} = 0.32$

$$\text{mode period} = \frac{2\pi}{s_i} = 11.8 \approx 37 \times \tau_{circ}$$

Bluestein (2003): $\tau_{circ} = \frac{2\pi \times \mathrm{RMW}}{V_{max}} = \frac{2\pi \times 200\mathrm{m}}{25\mathrm{m/s}} = 50\mathrm{s}$

$$\text{mode period} = 1 - 2 \text{ minutes} \approx 1 - 2 \times \tau_{circ}$$

Tanamachi (2007): $\tau_{circ} = \frac{2\pi \times \mathrm{RMW}}{V_{max}} = \frac{2\pi \times 60\mathrm{m}}{40\mathrm{m/s}} = 9\mathrm{s}$

$$\text{mode period} = 1 - 2 \text{ minutes} \approx 7 - 14 \times \tau_{circ}$$

But: Radar analyses smooth out RMW and underestimate V_{max}.

So real values of τ_{circ} may be much smaller, leading to a better match with the mode.

Summary

- Linearized stability analysis predicts the dominant asymmetric structures of a fully nonlinear simulation.

- The primary growth mechanism is extraction of energy from the vertical deformation of the flow - not the radial shear of tangential wind.

- Weakly unstable symmetric modes may explain symmetric oscillations that recently have been observed.

All the details and more can be found in:

J. Fluid Mech., page 1 of 40. © Cambridge University Press 2012 1
doi:10.1017/jfm.2012.369

Three-dimensional instabilities in tornado-like vortices with secondary circulations

David S. Nolan†

Rosenstiel School of Marine and Atmospheric Science, University of Miami, Miami, FL, USA

(Received 12 January 2012; revised 21 May 2012; accepted 17 July 2012)

Tornadoes and other intense atmospheric vortices are known to occasionally transition to a flow structure with multiple vortices within their larger circulations. This phenomenon has long been ascribed to fluid dynamical instability of the inner-core circulation, and many previous studies have diagnosed low-wavenumber unstable modes in tornado-like vortices that resemble the observed structures. However, relatively few of these studies have incorporated the strong vertical motions of the inner-core circulation into the stability analysis, and no stability analyses have been performed using a complete, frictionally driven secondary circulation with strong radial inflow near the surface. Stability analyses are presented using the complete circulations generated from idealized simulations of tornado-like vortices. Fast-growing unstable modes are found that are consistent with the asymmetric structures present in these simulations. Attempts to correlate the structures and locations of these modes with instability conditions for vortices with axial jets derived by Howard & Gupta and by Leibovich & Stewartson produce only mixed results. Analyses of perturbation energy growth show that interactions between eddy fluxes and the radial shear of the azimuthal wind contribute very little to the growth of the dominant modes. Rather, the radial shear of the vertical wind and the vertical shear of the vertical wind (corresponding to deformation in the axial direction) are the primary energy sources for perturbation growth. Relatively weak axisymmetric instabilities are also identified that have some similarity to symmetric oscillations that have been observed in tornadoes.

Symmetric Modes: Purely Real Eigenvalues

DVJ

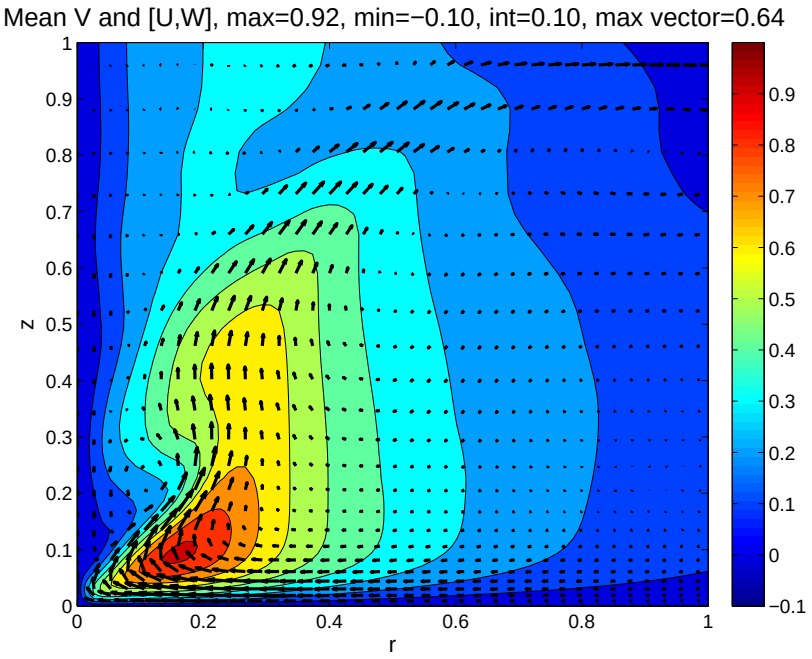

most unstable symmetric mode

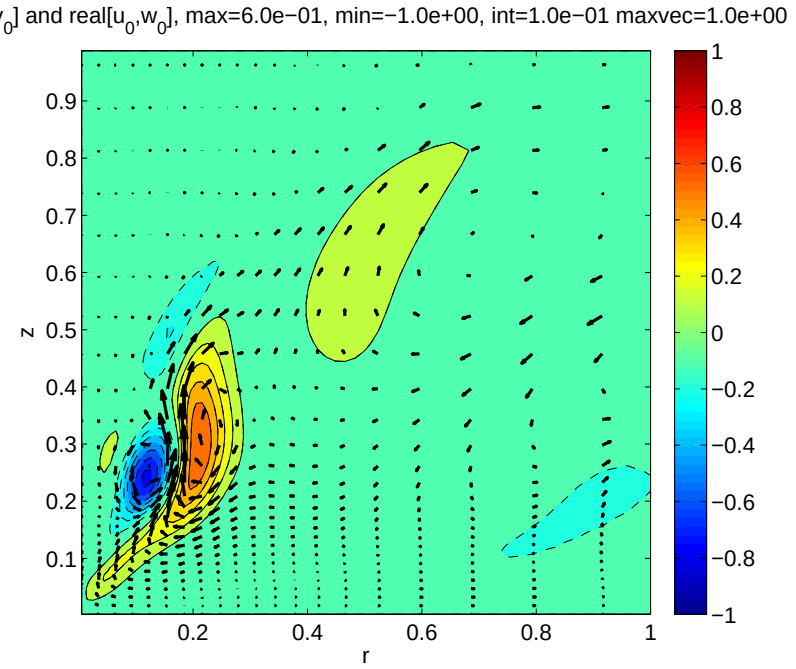

“stationary overturning”

- How do these modes change the mean flow?

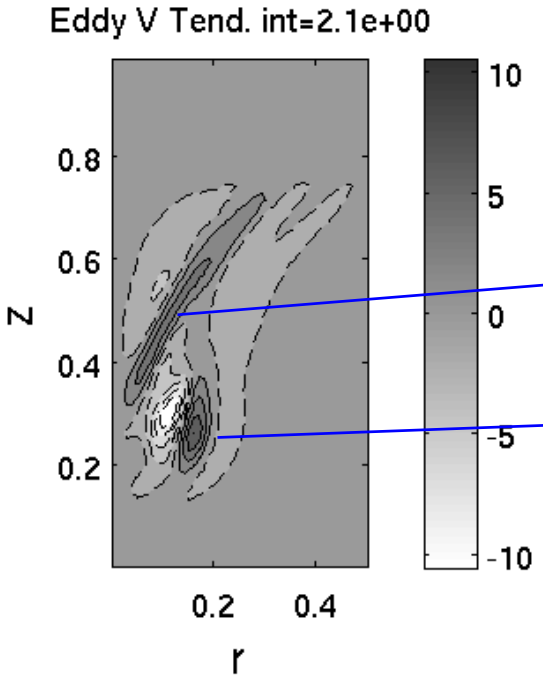

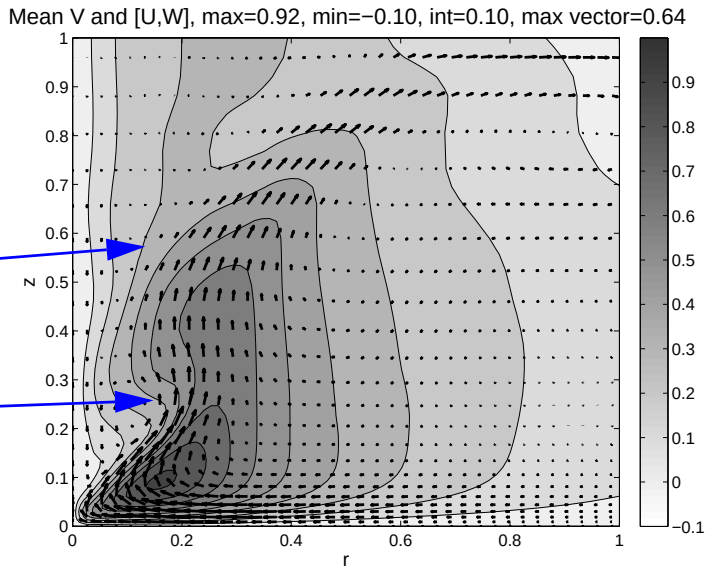

outflow aloft is filled in;
"notch" is smoothed out

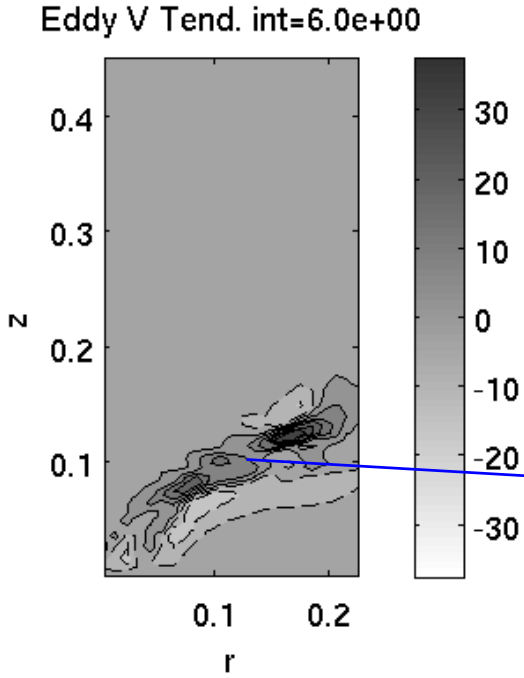

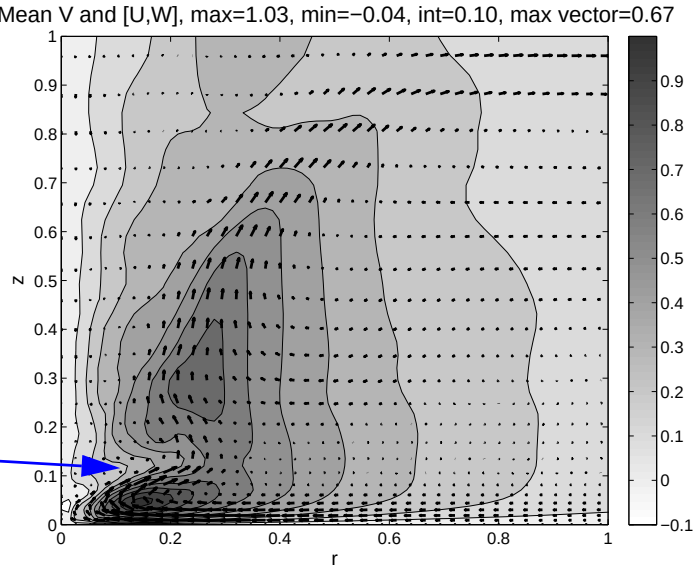

low-level jet is expanded upward